Manuscript Details

Manuscript number	HMT_2019_5714
Title	EFFECT OF COPPER FOAM THICKNESS ON POOL BOILING HEAT TRANSFER OF HFE-7100
Article type	Full Length Article

Abstract

Pool boiling is a low-cost technique for cooling electronic devices; HFE-7100 is a dielectric fluid with advantageous properties for such application but its high wettability can cause temperature overshoot in the system. Hence, the use of porous heating surfaces improves the heat transfer performance, eliminating the temperature overshoot due to their interconnected porous, which increase the wetted area and active nucleation site density. This work addressed pool boiling tests by using HFE-7100 and copper foams with three different thicknesses: 3 mm, 2 mm, and 1 mm in order to study the vapor bubble dynamics into the foam cell and find out an optimum thickness to enhance the boiling heat transfer. The results show that high thickness, 2 mm and 3 mm, has the best performance at low heat fluxes while the lowest thickness has the best performance at high heat fluxes. At heat fluxes lower than 50 kW/m², the higher surface wetted area increases the natural convection zone even though the latent heat also plays an important role. At higher heat fluxes, mainly after 200 kW/m², the vapor bubbles are trapped at the foam structure leading to an unstable boiling pattern and prevent the liquid from rewetting the surface. Therefore, the lowest foam thickness reduces the vapor trapping into the cell; additionally, the capillary-wicking ability increases and it also improves the HTC and the dryout heat flux due to the prevention of hotspots within the foam surface.

Keywords	pool boiling; HFE-7100; porous surface; copper foam; thickness.

Corresponding Author	Elaine Maria Cardoso
Corresponding Author's Institution	UNESP - Universidade Estadual Paulista
Order of Authors	Leonardo Manetti, Ana Moita, Reinaldo Rodrigues de Souza, Elaine Maria Cardoso
Suggested reviewers	

Submission Files Included in this PDF

File Name [File Type]

Cover Letter_IJHMT.pdf [Cover Letter]

Highlights.pdf [Highlights]

Graphical Abstract.pdf [Graphical Abstract]

Manetti_et_al_IJHMT_2019_Final.pdf [Manuscript File]

To view all the submission files, including those not included in the PDF, click on the manuscript title on your EVISE Homepage, then click 'Download zip file'.

Research Data Related to this Submission

There are no linked research data sets for this submission. The following reason is given:
Data will be made available on request

EFFECT OF COPPER FOAM THICKNESS ON POOL BOILING HEAT TRANSFER OF HFE-7100

Leonardo Lachi Manetti[1], Ana Sofia Oliveira Henriques Moita[2], Reinaldo Rodrigues de Souza[1] and Elaine Maria Cardoso[1]*

[1]*UNESP – São Paulo State University, School of Engineering, Post-Graduation Program in Mechanical Engineering, Av. Brasil, 56, 15385-000, Ilha Solteira, SP, Brazil*

[2]*IN+, Dep. Mechanical Engineering, Instituto Superior Técnico, Universidade de Lisboa, Lisbon, Portugal*

*Corresponding author: elaine.cardoso@unesp.br

Abstract

Pool boiling is a low-cost technique for cooling electronic devices; HFE-7100 is a dielectric fluid with advantageous properties for such application but its high wettability can cause temperature overshoot in the system. Hence, the use of porous heating surfaces improves the heat transfer performance, eliminating the temperature overshoot due to their interconnected porous, which increase the wetted area and active nucleation site density. This work addressed pool boiling tests by using HFE-7100 and copper foams with three different thicknesses: 3 mm, 2 mm, and 1 mm in order to study the vapor bubble dynamics into the foam cell and find out an optimum thickness to enhance the boiling heat transfer. The results show that high thickness, 2 mm and 3 mm, has the best performance at low heat fluxes while the lowest thickness has the best performance at high heat fluxes. At heat fluxes lower than 50 kW/m², the higher surface wetted area increases the natural convection zone even though the latent heat also plays an important role. At higher heat fluxes, mainly after 200 kW/m², the vapor bubbles are trapped at the foam structure leading to an unstable boiling pattern and prevent the liquid from rewetting the surface. Therefore, the lowest foam thickness reduces the vapor trapping into the cell; additionally, the capillary-wicking ability increases and it also improves the HTC and the dryout heat flux due to the prevention of hotspots within the foam surface.

Keywords: pool boiling, HFE-7100, porous surface, copper foam, thickness

Nomenclature

Alphabetic

A_c	Capillary tube area	[m^2]
a_{sf}	Specific area	[m^2/m^3]
c_p	Specific heat capacity	[J/kg·K]
C_{sf}	Surface-fluid coefficient	[-]
D_d	Bubble departure diameter	[m]
d_f	Fiber diameter	[m]
dh	Liquid column variation	[m]
d_p	Pore diameter	[m]
f_w	Heat surface material parameter	[-]
F	Inertia coefficient	[-]
h	Heat transfer coefficient	[W/m^2·K]
k_{Cu}	Copper thermal conductivity	[W/m·K]
K	Permeability	[m^2]
L	Copper block distances	[m]
L_b	Characteristic length	[m]
M	Molar mass	[kg/kmol]
m	Exponent of heat flux in Eq.(17).	
P	Pressure	[Pa]
Pr	Prandtl number	[-]
p_r	Reduced pressure	[-]
$q''_{measured}$	Heat flux measured at copper block	[W/m^2]
R_a	Average roughness	[μm]
R_{eff}	Effective pore radio	[m]
s	Gap size	[m]
$\dot{v}$	Wicked volume	[m^3]
T	Temperature	[K]
t	Time	[s]
u	Uncertainty	
u	Fluid velocity	[m/s]
y	Liquid rising height	[m]

Greek symbols

δ	Foam thickness	[m]
ΔT	Temperature difference	[K]
ε	Porosity	[-]
θ	Static contact angle	[degree]
σ	Surface tension	[N/m]
μ	Viscosity	[kg/m·s]
ρ	Density	[kg/m^3]
ρ_{foam}	Foam density	[kg/m^3]
ρ_{Cu}	Copper density	[kg/m^3]
ρ_r	Relative density	[-]

Subscripts

1, 2, or 3	Thermocouples position
atm	Atmospheric condition
l or liq	Liquid fluid condition
s	Surface square cross-section
sat	Saturation fluid condition
vap	Vapor fluid condition
w	Surface wall

1. Introduction

It is well known that microelectronics and microchips have been increasing in power, also in heat generation, but decreasing in size [1]. Efficient thermal management solutions are crucial to maintaining new electronic devices within the operating temperature limits [2]. Immersion cooling with two-phase change – pool boiling – is a low-cost technique because it works with passive fluid circulation, is easy to construct, and requires low maintenance. Consequently, pool boiling has been used as a way of reaching the power dissipation needed by electronic devices [3]. Another pool boiling advantage is the component-liquid direct contact that eliminates the contact resistance; however, liquids with high electric conductivity, *i.e.*, water cannot be used. For this reason, the fluorochemical fluids such as fluorocarbons (FCs) and hydrofluoroethers

(HFEs) are advantageous due to their dielectric and inert properties, nonflammable and non-reactive characteristics, *i.e*. they are chemically compatible [4]. Besides that, FC-72 and HFE-7100 have a low boiling point, $T_{sat} \approx 60$ °C at 1 atm, which maintains the electronic components at low operating temperatures, < 85 °C [5 - 7]. In addition, both are chlorine free fluids that provide an ozone depleting potential, ODP = 0; on the other hand, HFE-7100, has superior environmental properties due to its global warming potential, $GWP_{100} = 320$ [8], while FC-72 has a $GWP_{100} > 5000$ [9].

Pool boiling system is limited by the critical heat flux (CHF) and heat transfer coefficient (HTC) values caused by a counterflow of vapor and liquid flow during the process [10]. One promising way to enhance the CHF and HTC is to modify the heating surface morphology [11]. Porous surface structures have been widely reported to enhance heat transfer performance due to their interconnected porous, which increase the wetted area and the nucleation site density [12]. The porous thickness and pore size are the two most important parameters of a porous surface, and their optimal values mainly depend on the fluid properties [13]. One example of a porous surface is the open-cell metal foams, which are surfaces with high porosity ($\varepsilon > 80\%$) composed by tetradecahedron foam cells [14]. According to Zhao (2012) [15], these metal foams have high surface area density (>1000 m^2/m^3) and low-cost manufacturing process.

Researchers have been studying experimental works in pool boiling using metal foams. Atherya et al. [16] studied aluminum metal foam on FC-72 with different thicknesses (2.3 mm – 25.4 mm) and different pores per inch (PPI). They reported that the first vapor bubbles grew in the junction surface-foam and as the heat flux increases the bubbles within the structure also increase. Thicker foams enhance the HTC at first heat fluxes while the lowest thickness had the highest CHF.

Xu et al. [17] used acetone as working fluid on copper foam with three different porous densities 30, 60, and 90 PPI at a constant thickness ($\delta = 3$ mm). All foams presented negligible wall temperature excursion at boiling incipience. The authors reported an HTC and CHF enhancement due to the high liquid contact area, more density of active sites, and capillary-assist liquid flow towards foam cells. Yang et al. [18] used the Xu et al. [17] methodology and surfaces; however, they used water as working fluid and different foams thickness – from 1 mm to 5 mm. They found out that the HTC enhancement on the metal foams depends on the balance between the liquid suction capability towards the porous structure and the vapor release resistance to the bulk liquid. The optimum thickness decreases as the porous density increases because

high porous density increases the surface area and consequently the nucleation sites; however, it decreases the bubbles release resistance.

Xu and Zhao [19] investigated the saturated pool boiling heat transfer of deionized (DI) water on a copper foam surface with V-shape grooves and reported that large foam thickness can offer a high surface area although creates considerable resistance for bubble escape; thus, grooves in the foam structure could help the vapor bubbles escape. Additionally, Xu and Zhao [20] studied DI water on pool boiling of gradient metal foams, with a foam of high porous density at the lower lever and low porous density at the upper level; according to the authors, the low porous density delays the bubble departure and increase the bubble growing time, which helps the HTC enhancement while the high density increase the nucleation sites.

Recently, Zhou et al. [21] used copper foams with 10, 50, and 110 PPI on pool boiling of DI water with and without n-butanol solution at 6 wt.%. The metal foams were observed to increase the HTC, as porous density increased, for both fluids. In addition, for high heat fluxes, the n-butanol solution decreases the surface tension and, as a consequence, the vapor bubbles evacuation is promoted.

Finally, Wong and Leong [22] printed a homogeneous metal foam structure by using Selective Laser Melting (SLM) in order to study the effect of porous diameter and foam thickness on pool boiling of FC-72. They concluded that porous structures increase the bubble nucleation site density due to the larger surface area and capillary-assisted liquid suction which allow better liquid replenishment; however, a larger surface area corresponds to an increase in the form drag and, consequently, in the bubble evacuation resistance. The bubble evacuation resistance increases for higher heat flux and structure height and for smaller unit cell size.

Based on the previous literature review, in fact, the metal foams increase the HTC and the CHF as compared to plain/flat surfaces. The main effect reported is the wetted area enhancement that promotes bubbles formation at low heat fluxes coupled with more nucleation sites at high heat fluxes; moreover, as the foam PPI increases, the wetted area also increases and the pore diameter decreases. Small pores increase the capillary-assist liquid flow towards foam cells; on the other hand, small pores make the bubble vapor evacuation difficult at high heat fluxes. Finally, thicker foams had greater wetted area and improve the HTC at low heat fluxes while deteriorates the heat transfer performance at high heat fluxes due to the thermal resistance created by the vapor

within the porous structure. However, the effect of foam thickness is not clear for wetting fluids such as HFE-7100.

This paper presents an experimental work on pool boiling using HFE-7100 (at saturated conditions) and metal foams of copper (Cu) at three different thicknesses (δ): 3 mm, 2 mm, and 1 mm. The present work aims to: (i) increase the database of fluid-surface combinations; (ii) understand the vapor bubble dynamics into the foam cell by using high-speed camera images and liquid flow by wickability analysis; (iii) find out a foam optimum thickness to enhance the boiling heat transfer with dielectric fluid.

2. Surface preparation and characterization

2.1 Foams parameters

The open cell copper metal foam was purchased from Nanoshel® as a $500 \times 500\ mm^2$ sheet with a 3 mm thickness. It was fabricated by using metal deposition in a cellular preform as detailed by Ashby et al. [23] and Bahart [24]. First, the pane was cut in squares of $16 \times 16\ mm^2$ (Fig. 1) by using electrical discharge wire cutting (wire EDM) [25].

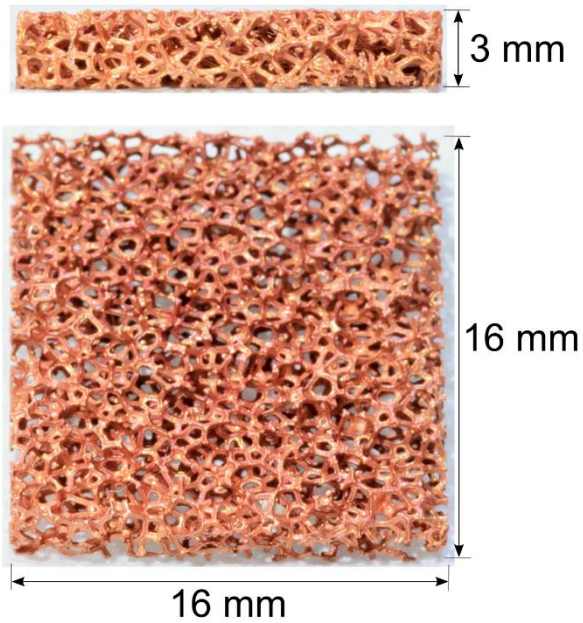

Figure 1. Copper foam section.

The porosity (ε) was obtained by weighing seven samples with the same size in an analytical balance and comparing the foam density, ρ_{foam}, with the copper density,

$$\varepsilon = 1 - \rho_r = 1 - \frac{\rho_{foam}}{\rho_{Cu}} \quad (1)$$

Moreover, the following methods were used to characterize the copper foam: (i) optical images using a stereo microscopy Zeiss® SteREO Discovery.V8 and scanning electron microscopy (SEM) by using an EVO LS15 Zeiss®, Fig. 2; (ii) X-ray microcomputed tomography (µCT) by using a Skycan 1272 at a resolution of 15 µm (100 kV X-ray source voltage); and (iii) wickability based on the wicked volume in a capillary tube (1 mm diameter), section 2.3.

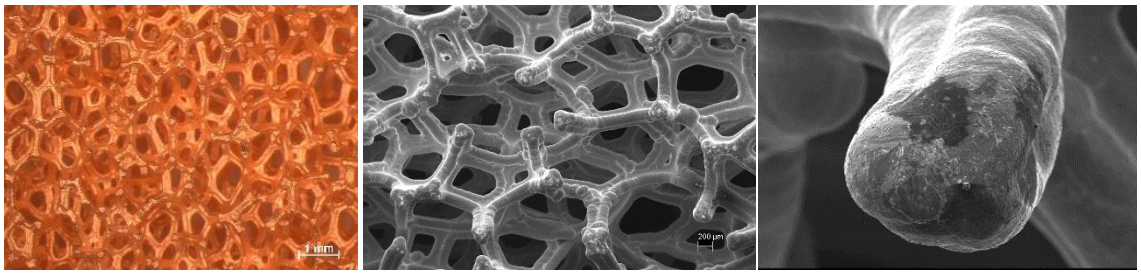

(a) (b) (c)

Figure 2. Copper metal foam images: (a) Stereo top view; (b) SEM top view; and (c) SEM fiber cross section.

In order to perform the PPI measurement, using the images, seven lines in each direction were traced and the number of porous which intercepted lines was counted; thus, an average of each direction line was calculated and the average of the two direction yields the PPI of the open-cell metal foam. The average PPI value was 31.75 with a standard deviation of 6.2. In addition, the µCT images were used for measuring the foam porous diameter and fibers diameters (d_p and d_f, respectively), and the specific area (a_{sf}). First, the µCT virtual slices were input in the imoph software [26] in order to measure the surface granulometry by using the aperture map function for both phases (solid and porous) as explained by Vicente et al. [27]. Figure 3a shows the histogram and the normal distribution that allows defining a mean pore diameter, which is shown in Table 1. The µCT virtual slices were input in the vmtk® software for measuring the specific area; vmtk uses the 'marching cubes' algorithm to extract the interface between

the porous and solid phases by creating a triangulated surface mesh that is rendered to form a solid (Figure 3b). In order to distinguish the two phases, a grayscale threshold value was selected such that the porosity of the reconstructed 3D volume matched with the measured foam porosity (Table 1) as explained by Sarangi et al. [20]. After setting the correct grayscale, the area density was obtained by the ratio between the surface solid area (foam area) and its total volume (solid volume + porous volume) as showed in Table 1.

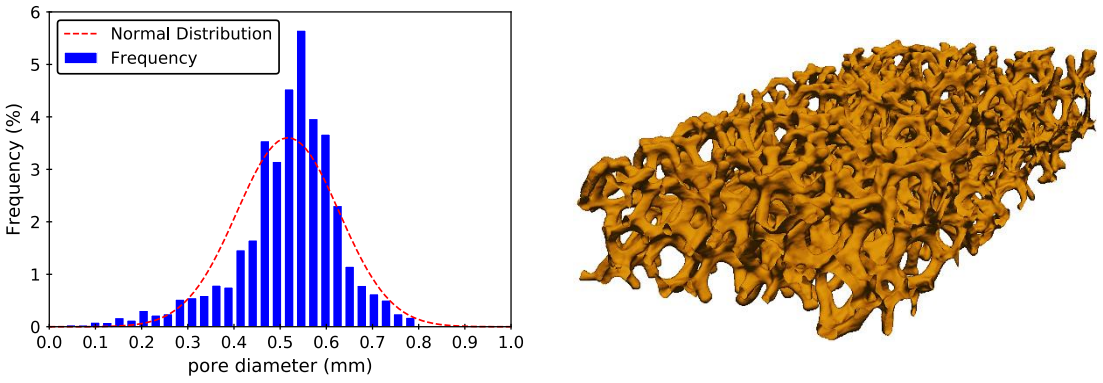

(a) (b)

Figure 3. Copper foam: (a) pore diameter distribution and (b) Rendered tridimensional surface.

Table 1. Copper foam characteristics.

Weight ($kg \times 10^{-3}$)	ρ_{foam} (kg/m^3)	ρ_r [1] (%)	ε (%)	d_p (mm)	d_f (mm)	a_{sf} (m^2/m^3)
0.697	908.1	10.1	90.0	0.52	0.1	2166

[1]Pure material density: ρ_{Cu} = 8960 kg/m^3.

2.2 Foam thickness variation

The copper foams with 3 mm in thickness were welded (soldering process [25]) on the copper block with a plain and square plate on the upper surface (16 × 16 × 3 mm^3) of the copper cylinder. (Fig. 4). In order to ensure small thermal resistance between the foam and the test section, a thin tin layer (0.1 mm thickness) was applied between the plain surface and the copper foam; after that, the copper block was heated by a cartridge resistance up to the tin alloy melting point (≈ 200 °C) and a weight was put on the foam

to pressure it against the plain surface. Finally, the assembly was cooled and cleaned with alcohol and acetone.

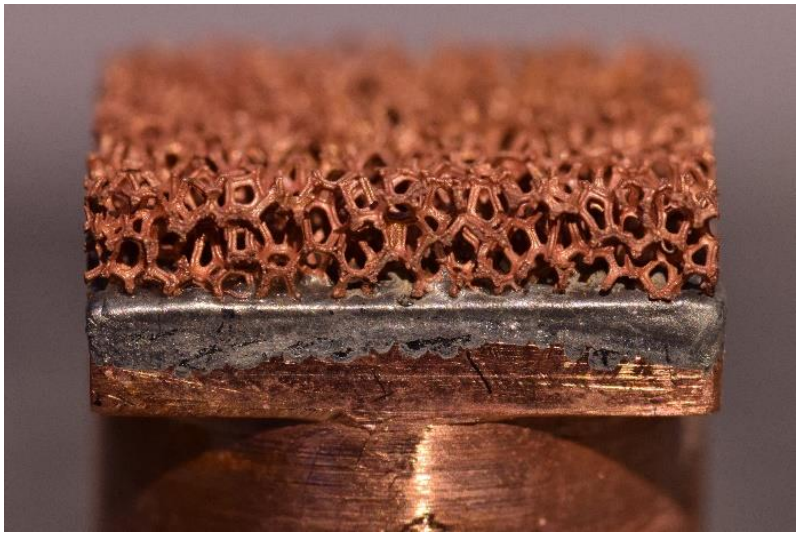

Figure 4. Copper foam 3 mm soldered on the plain copper block.

Furthermore, more two foam thicknesses were used in this work. For the thickness level variation was used the electric discharge machining process (EDM), where a square flat copper block (20×20 mm^2) was used as an electrode tool as shown in Fig. 5a. Figure 5b shows the copper foam after machining with δ =1 mm.

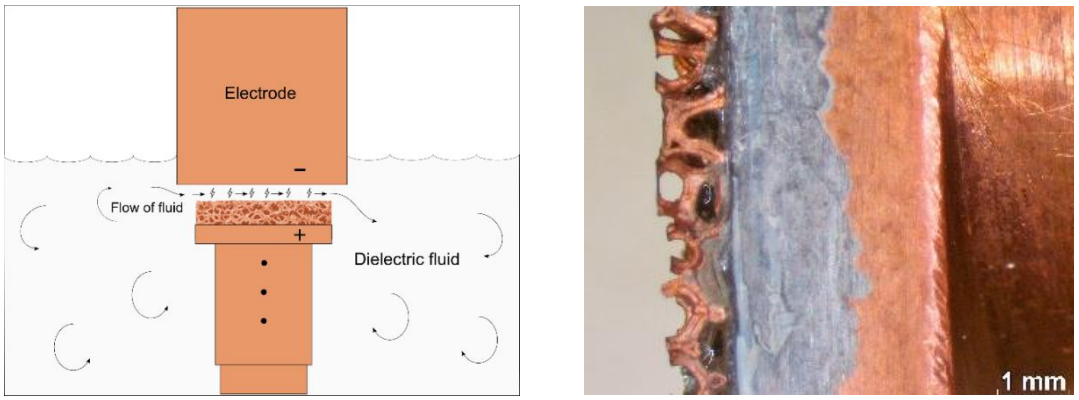

(a) (b)

Figure 5. Foam thickness level variation. (a) EDM basic setup; (b) metal foam after the machining process.

2.3 Wickability analysis

The previous works on metal foams [17 - 19, 21] refer to the capillary-assist as one of the main effects of the enhancement in the HTC and CHF. They based their analysis on Young-Laplace equation for a capillary tube,

$$\Delta P = \frac{2\sigma \cos\theta}{d_p} \tag{2}$$

by considering the interconnected pores as capillary tubes; therefore, smaller pore diameter resulted in a larger capillary driving pressure, which should improve liquid replenishment [21].

Other researches on porous surfaces have used techniques to quantify the surface wickability. For instance, Nam et al. [29], Ahn et al. [30], Gheitaghy et al. [31] and Wang et al. [32] performed the capillary rate-of-rise experiment where the porous surface stayed oriented perpendicular to a horizontal liquid reservoir. Once the sample bottom touches the reservoir surface, the liquid rises along the surface due to a finite capillary pressure gradient. The liquid rising height is tracked by a high-speed camera and, according to the Washburn's equation, for capillary structures of small effective pore diameters (lower than 300 μm), the square of liquid rising height (y^2) has a linear correlation with the rising time (t),

$$y^2 = \left(\frac{2\sigma}{\varepsilon\mu}\right)\left(\frac{K}{R_{eff}}\right)t \tag{3}$$

When the effective pore radio (R_{eff}) decreased, the capillary pressure increased; on the other hand, permeability (K) is going to decrease as a penalty.

Similarly, Ahn et al. [33], Rahman et al. [34], Cao et al. [35] and Cao et al. [36] carried out capillary-wicking tests where the porous surface is slowly raised to contact a pendant fluid droplet attached to a small diameter capillary tube. As the surface makes contact with the droplet, the liquid is wicked into the porous structure and the volumetric flow rate is measured by monitoring the liquid meniscus in the tube. The wickability is characterized by the absorbed flow rate defined as,

$$\dot{V} = A_c\left(\frac{dh}{dt}\right)_{t=0} \tag{4}$$

where A_c is the capillary tube area and dh is the liquid column variation inside the capillary tube.

As our copper foams samples have a porous diameter higher than 300 µm, the capillary-wicking test previously presented was chosen to compare the wickability of the copper foams with different thicknesses. The capillary tube used had 1 mm in diameter. The schematic experimental layout is shown in Fig. 6a and the liquid absorption on 'Cu foam 3 mm' in Fig. 6b. Figure 7 shows the volume wicked by all surfaces tested for the first 30 milliseconds, where the straight lines represent the initial wicked volume. One may observe that the ability to absorb the liquid increases as the thickness decreases.

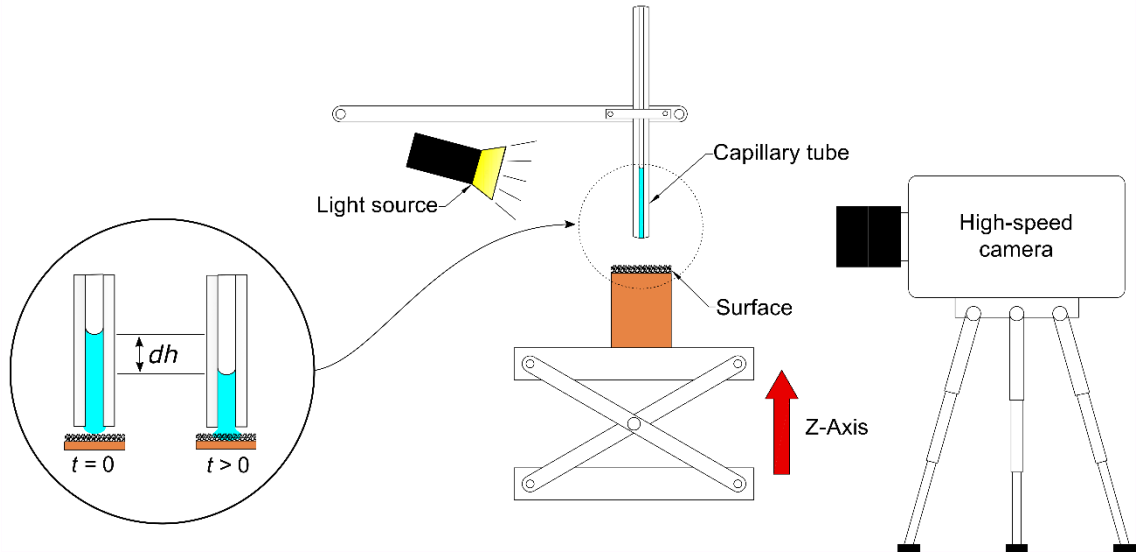

(a)

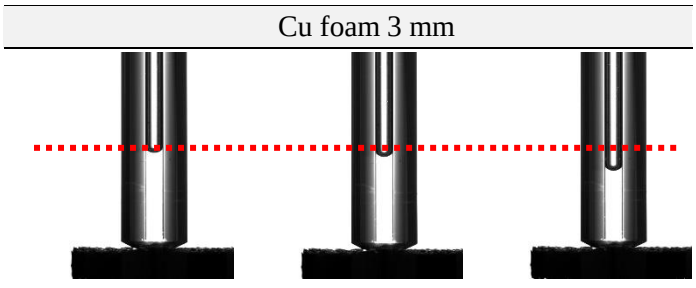

(b)

Figure 6. Wickability analysis: (a) Schematic of the experimental device used for the wickability measurements (b) Metal foams capillary wicking for 3 mm.

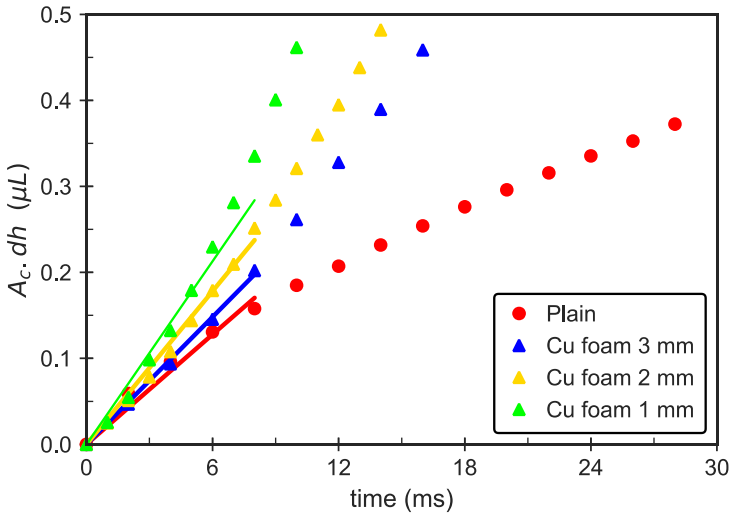

Figure 7. Volume wicked by all surfaces tested.

3. Experimental setup and data reduction

The pool boiling tests were performed in the apparatus (Fig. 8) that consists of a rectangular glass (120 × 100 mm²) with a thickness of 5 mm and 200 mm height. The upper and lower bases consisted of two stainless steel plates, 200 × 200 × 10 mm³. The required tightness was obtained with nitrile rubber insulation and silicone. A thermal bath, operated with water, was used to control the condenser temperature located at the top of the boiling chamber. An auxiliary heater – a cartridge resistance with a maximum power of 250 W at 220 V submerged in the working fluid – was used to maintain the liquid temperature near the saturation point since the power was controlled with a variable transformer. Two K-type thermocouples, $T_{liq,}$ and T_{vap}, located in the working fluid and vapor, respectively, allowed monitoring the test condition temperature. The pressure inside the boiling chamber was measured by a pressure transducer Omega PXM309-2A and maintained close to the local atmospheric pressure, p_{atm} = 98 kPa, during the boiling tests. The pressure uncertainty, certified by Omega, is ± 0.05 kPa.

The test section, Fig. 9, consisted of a copper piece with a square plate on the upper surface (16 × 16 × 3 mm^3) of the copper block with 16 mm diameter and 60 mm height. Three K-type thermocouples (T_1, T_2, and T_3) with 0.5 mm diameters were used to estimate the wall temperature (T_w) and the heat flux ($q''_{measured}$). A cartridge resistance, with a maximum power of 300 W at 220 V, heated the bottom part of the copper block; the power was supplied by a stabilized variable DC power source. The thermal

insulation of the test section consisted of polytetrafluoroethylene (PTFE). In order to eliminate the natural parasite sites at the interface PTFE-test section surface, a two-component epoxy resin was used to fill the gap (Fig. 10).

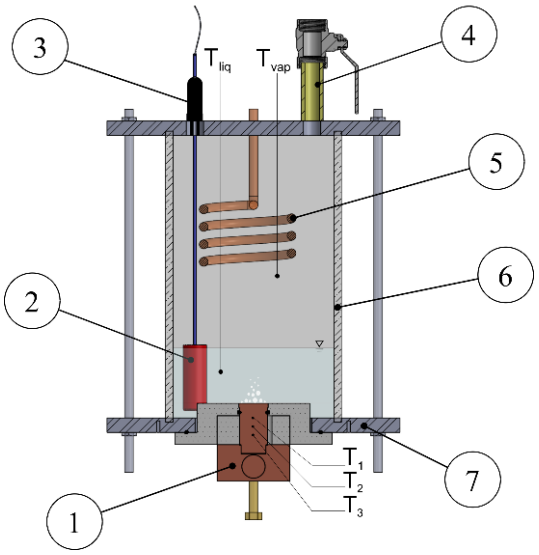

Figure 8. Pool boiling apparatus: (1) cooper block; (2) auxiliary heater; (3) pressure transducer; (4) vacuum/feed valve; (5) condenser; (6) glass chamber; (7) stainless steel plate.

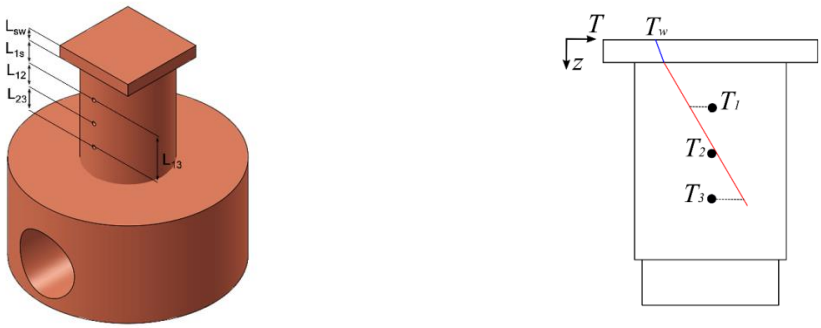

(a) (b)

Figure 9. Test section view: (a) distance between the thermocouples and the surface wall; (b) temperature linear profile in both cross-sections.

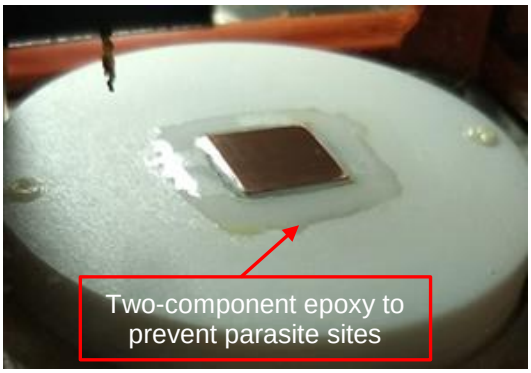

Figure 10. Plain heating surface with epoxy on the surface border.

The boiling tests were performed by using HFE-7100 (3M^{TM} Novec^{TM}) at saturated conditions – physical properties are listed in Table 2. A plain surface was tested and considered as a reference surface. As HFE-7100 has an extremely small contact angle (< 10°) [4], the plain surface (Ra = 0.14 μm) was prepared by sandpaper 600 grit in order to produce a rough surface as presented by Manetti et al. [37].

Table 2. Thermophysical properties of HFE-7100 at saturated conditions [8, 38].

Saturation pressure	T_{sat} (°C)	ρ_l (kg/m³)	ρ_v (kg/m³)	$10^6 \times \mu_l$ (Pa·s)	$c_{p,l}$ (J/kg·K)	h_{lv} (kJ/kg)	k_l (W/m·K)	σ (mN/m)
1 atm	61.0	1418	9.7	426.8	1255.0	111.6	0.069	10.20
98 kPa[a]	60.3	1420	9.5	430.5	1253.6	111.9	0.069	10.26

[a]Ambient pressure in Ilha Solteira, Brazil.

A vacuum was created to feed the chamber with the working fluid. Before each run, the auxiliary heater boiled the working fluid by 1 hour for degassing it. The test conditions were adjusted by monitoring the pressure and the temperature inside the boiling chamber. For each metal foam test, the experiment was carried out at least twice under similar conditions to ensure that the results were repeatable.

A data acquisition system (Agilent 34970A) acquired all data signals (voltage, pressure, and temperature). The applied heat flux was compared to the measured heat flux by using Fourier's law of conduction through the three thermocouples in the copper block,

$$q''_{measured} = \frac{\pi}{4} \cdot k_{Cu} \cdot \frac{\Delta T_{13}}{L_{13}} \tag{5}$$

where π/4 is due to the square cross-section at the surface upper level; L_{13} is the thermocouples distance, as shown in Fig. 9, equal to 12 mm.

The HTC was calculated using Newton's law of cooling given by:

$$h = \frac{q''_{measured}}{T_w - T_{sat}\,(p_{int})} = \frac{q''_{measured}}{\Delta T_{sat}} \tag{6}$$

where $T_{sat}(p_{int})$ corresponds to the saturation temperature of the HFE-7100, at pressure inside de boiling chamber, given by [8]:

$$\ln P_{sat}(\text{at Pascal}) = -\frac{3641.9}{T_{sat}(\text{at Kelvin})} + 22.415 \tag{7}$$

and T_w is the wall temperature given as follows:

$$T_w = T_1 - \frac{q''_{measured}}{k_{Cu}} \cdot \frac{4}{\pi} L_{1s} - \frac{q''_{measured}}{k_{Cu}} \cdot L_{sw} \tag{8}$$

where the second term is the linear temperature profile at the end of the circular section (L_{1s} = 5 mm) and the third term is the linear temperature profile in the square section (L_{sw} = 3 mm), as shown in Fig. 9.

The experimental uncertainties (u) were calculated by using the method described by Moffat [39] where the uncertainty in the result R is a function of the independent variables X_i as follow:

$$u_R = \left[\left(\sum_i^n \frac{\partial R}{\partial X_i} u_{X_i} \right)^2 \right]^{\frac{1}{2}} \tag{9}$$

Therefore, the relative uncertainty for the heat flux between the thermocouples 3 and 1 was given by:

$$\frac{u_{q''_{measured}}}{q''_{measured}} = \left[\left(\frac{u_{\Delta T_{13}}}{\Delta T_{13}} \right)^2 + \left(\frac{u_{L_{13}}}{L_{13}} \right)^2 \right]^{1/2} \tag{10}$$

where the differential uncertainty of the K-type thermocouples was ± 0.3 °C (corresponds to the thermocouples uncertainties after the calibration); the uncertainty in

the position of the thermocouple junction was estimated to be ± 0.03 mm, and the wall superheat uncertainty was given by:

$$u_{\Delta T_{sat}} = \left[u_{T_1 - T_{sat}}^2 + \left(\frac{-(4/\pi) \cdot L_{1s} - L_{sw}}{k_{Cu}} u_{q''_{measured}} \right)^2 + \left(\frac{-(4/\pi) \cdot q''_{measured}}{k_{Cu}} u_{L_{1s}} \right)^2 + \left(\frac{q''_{measured}}{k_{Cu}} u_{L_{sw}} \right)^2 \right]^{1/2} \quad (11)$$

Finally, the HTC uncertainty was given by:

$$\frac{u_h}{h} = \left[\left(\frac{u_{\Delta T_{sat}}}{\Delta T_{sat}} \right)^2 + \left(\frac{u_{q''_{measured}}}{q''_{measured}} \right)^2 \right]^{1/2} \quad (12)$$

Therefore, the experimental uncertainty of the heat transfer coefficient is higher in low heat fluxes while it decreases as heat fluxes are increased. For all surfaces tested, the experimental uncertainty for the heat flux and the heat transfer coefficient varied from 18.3 to 3.3 % and from 18.4 to 3.8 %, respectively.

4. Results and Discussion

4.1 *Validation of the experimental apparatus*

In order to verify the pool boiling apparatus accuracy, tests were carried out for HFE-7100 on the plain surface and the experimental values were compared with the predictive correlations (Fig. 11). First, it was used the well-known Rohsenow's correlation [40],

$$\frac{c_{pl} \Delta T_{sat}}{h_{lv}} = C_{sf} \left[\frac{q''}{\mu_l h_{lv}} \sqrt{\frac{\sigma}{g(\rho_l - \rho_v)}} \right]^{1/3} Pr_l^{1.7} \quad (13)$$

that can be rewritten changing $\Delta T_{sat} = q''/h$,

$$h = \frac{1}{C_{sf} Pr_l^{1.7}} \frac{q'' c_{pl}}{h_{lv}} \left[\frac{\mu_l h_{lv}}{q''} \sqrt{\frac{g(\rho_l - \rho_v)}{\sigma}} \right]^{1/3} \quad (14)$$

where μ_l, h_{lv}, c_{pl}, and Pr_l correspond to the viscosity of the liquid (kg/m.s), the latent heat of vaporization (J/kg), the specific heat of the liquid (J/kg.K), and the Prandtl number of the liquid, respectively; in addition, σ is the liquid surface tension, ρ_l, and ρ_v are the liquid and vapor densities, respectively, g is the gravitational acceleration. C_{sf} is a coefficient that depends on the material of the heating surface and the surface finishing. The thermophysical properties of the HFE-7100 were obtained at p_{sat} = 98 kPa.

Moreover, it was used the Kiyomura et al. [41] correlation given by,

$$\frac{hL_b}{k_l} = 154 \left[\left(\frac{c_{pl} T_{sat}}{h_{lv}} \right)^{1.72} \left(\frac{c_{pl} \mu_l}{k_l} \right)^{-0.34} \left(\frac{D_d q''}{\mu_l h_{lv}} \right)^{0.62} \left(\frac{s}{L_b} \right)^{-0.05} \right] \quad (15)$$

where D_d is Fritz's model [42] for bubble departure diameter given by,

$$D_d = 0.0208 \cdot \theta \cdot L_b \quad (16)$$

and L_b is the characteristic length given by $L_b = \sqrt{\frac{\sigma}{g(\rho_l - \rho_v)}}$; k_l is the fluid thermal conductivity. The parameter s is the gap size for confining boiling test; so, as the present work does not have a confining element, s was the fluid column above the heating surface (s = 50 mm).

Ribatski and Jabardo [43] proposed an empirical correlation to estimate the boiling heat transfer in terms of reduced pressure (p_r). Their correlation was based on the experimental data for saturated pool boiling of halocarbon refrigerants on cylindrical surfaces of different materials:

$$h = f_w p_r^{0.45} (-\log p_r)^{-0.8} M^{-0.5} R_a^{0.2} q''^m \quad (17)$$

where $m = 0.9 - 0.3 p_r^{0.2}$ and f_w is the heat surface material parameter, equal 100 to copper, M and R_a represent the molar mass of the working fluid, and average surface roughness, respectively.

Finally, the curve fitting based on the relation between the heat transfer coefficient and the heat flux proposed by Stephan [44] is used to validate the experimental results:

$$h = Cq''^{n} \quad (18)$$

where C is a coefficient that depends on the surface-fluid interaction, and n is an exponent of the heat flux.

The predicted values agree well with the experimental data with a mean absolute percentage error (MAPE) of 10% for Rohsenow's correlation [40] by using a C_{sf} = 0.005, as suggested by Cao et al. [45]; 12% for Kiyomura et al. [41] by using the static contact angle, θ, equal to 2 degree; and, 10 % for Ribatski and Jabardo [43] correlation. The exponent n obtained by Stephan [44] fitting was around 0.7, agreeing with the value that generally lies between 0.6 and 0.8.

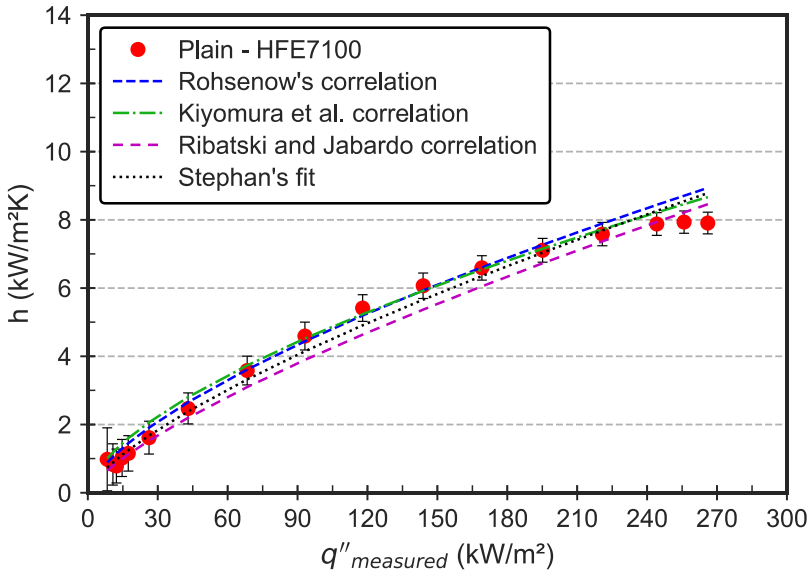

Figure 11. Pool boiling apparatus validation with HFE-7100.

4.2 *Copper foams pool boiling curves*

The boiling curves for metal foams and plain surface are shown in Fig. 12a and Fig. 12b shows the HTC curves. The results for plain surface were included for reference.

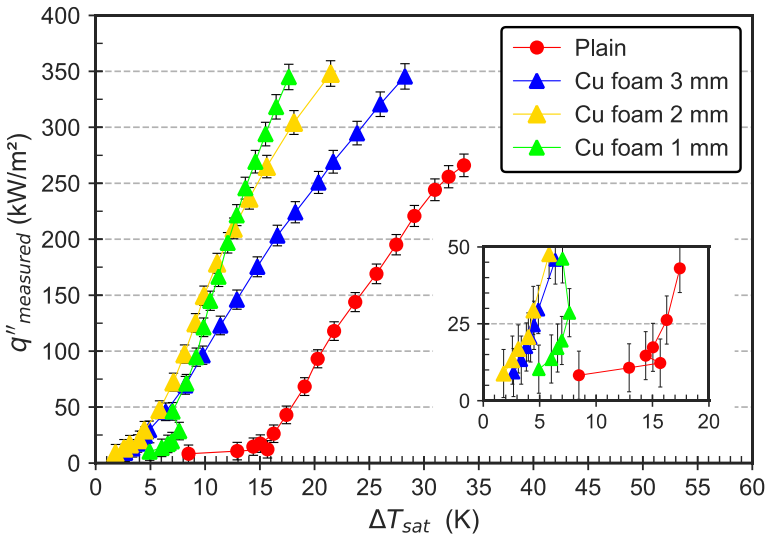

(a)

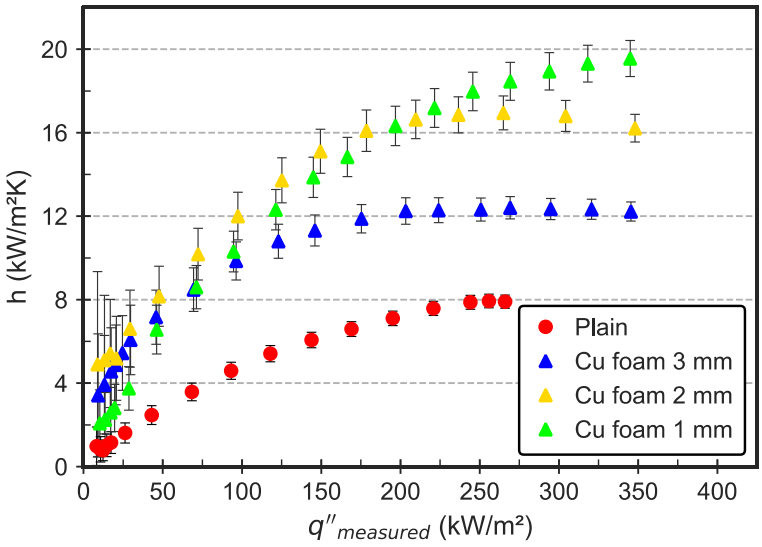

(b)

Figure 12. (a) HFE-7100 pool boiling on copper foams at saturated conditions and (b) HTC curves.

While the plain surface stayed just on natural convection at the first three heat fluxes of the boiling curve and showed a boiling incipience overshoot, the copper metal foam eliminated the thermal overshoot at the onset nucleate boiling (ONB), with some nucleation sites being activated at the first heat fluxes (≈10 kW/m²).

For q'' < 50 kW/m², the first two foams, δ = 2 mm and δ = 3 mm, showed no significant difference between them. In this way, even that copper has high thermal conductivity (k_{Cu} ≈ 400 W/m.K) and the foam with higher thickness had a greater

wetted area, the temperature drop through the copper foam plays a key role in the first heat fluxes and then thickness higher than 2 mm is not useful to heat transfer. Moreover, 'Cu foam 1 mm' presented the worst performance due to the lowest wetted area. Therefore, although all foams showed active sites at first heat flux, the natural convection also acts during the heat flux range < 50 kW/m² and influences the foams boiling curve.

As the heat flux increased, the thickness effect became more evident. For 50 kW/m² < q'' < 200 kW/m² there is fully developed nucleate boiling and the 'Cu foam 2 mm' remained with the best boiling performance while the 'Cu foam 3 mm' boiling curve starts to deviate to the right side, deteriorating the HTC; in contrast, the foam with δ = 1 mm change the curve slope, increasing its heat transfer performance.

In order to show more clearly the HTC enhancement effect of the foam, the experimental results were evaluated by using the heat transfer enhancement ratio, which is given by the ratio between the foam HTC and plain HTC as shown in Fig. 13.

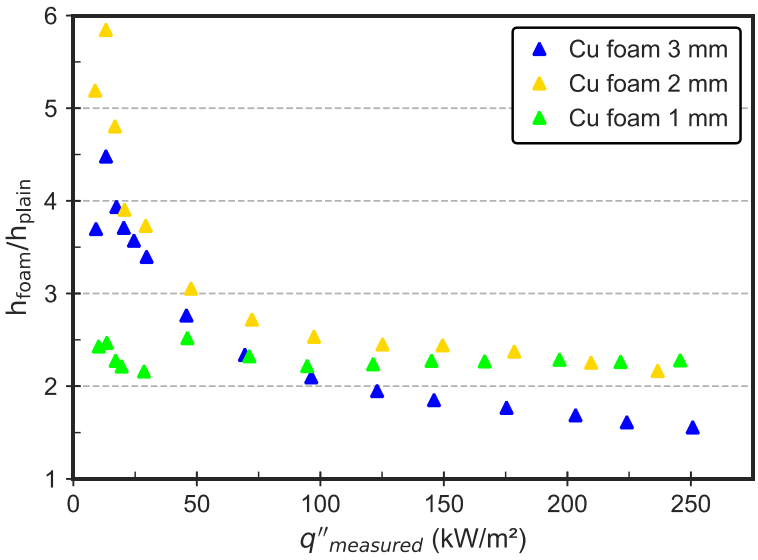

Figure 13. Pool boiling heat transfer coefficient enhancement ratio as a function of heat flux.

Figure 13 confirms the best performance of δ = 2 mm for heat fluxes q'' < 200 kW/m² but it has a slope downwards as the δ = 3 mm for q'' > 200 kW/m² while the δ = 1 mm remained a ratio almost constant close to 2.3 that imply an HTC average increase of 130 %. However, as the dryout heat flux for the plain surface was

close to 250 kW/m² and the maximum heat flux applied was 270 kW/m², the HTC ratio analysis cannot be carried out for the entire foam curves.

For an imposed heat flux $q'' > 200$ kW/m², the bubble frequency and coalescence increase within the foam structure. Therefore, as higher the foam thickness, higher is its bubble evacuation resistance; in other words, the foam structure traps vapor bubbles in the cell structure, leading to an unstable boiling pattern, which inhibits the cooling, effect and increases the wall temperature. Therefore, the lowest thickness showed the best result at high heat fluxes because even though the wetted area decreased, two other effects are pronounced: the vapor bubbles grow and rise easily and, the wickability effect increases (as shown in Fig. 7, section 2.3) *i.e.*, it has large capacity for pumping liquid to the hotspots. Figure 14a shows the relation between the maximum HTC reached by the metal foams and the maximum HTC reached by the plain surface and Figure 14b shows the relation between the metal foam dryout heat flux and the plain dryout. As can be seen, 'Cu foam 1 mm' has the best performance when critical/turning points are compared on both analysis; on the other hand, 'Cu foam 2 mm' was able to reach a higher HTC however, the heat flux turning point was very close to the 'Cu foam 3 mm' and plain one.

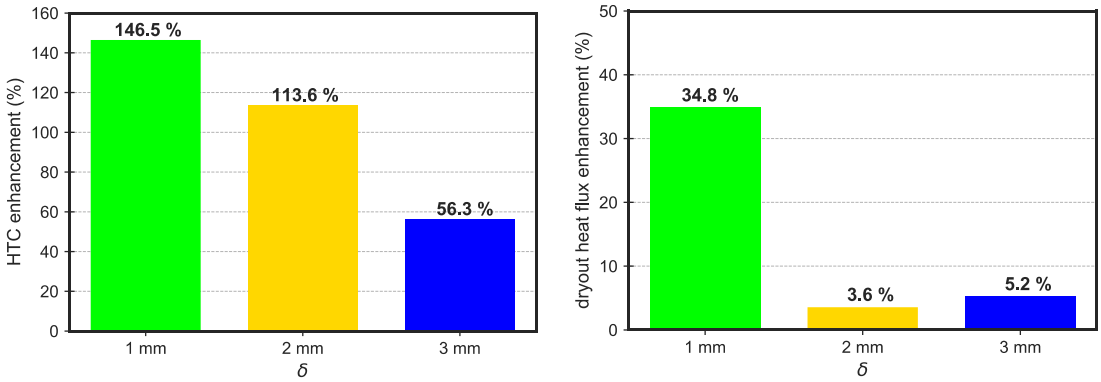

(a) (b)

Figure 14. (a) Maximum HTC enhancement for Cu foam (b) dryout heat flux for Cu foam.

In order to obtain an optimum thickness for each range of heat flux, the results were plotted as a function of the foam thickness at constant heat flux lines as shown in Fig. 15. The minimum superheating value and the maximum HTC value were found by

fitting a second-degree polynomial with a least-square method with all curves fit with $R^2 > 0.99$.

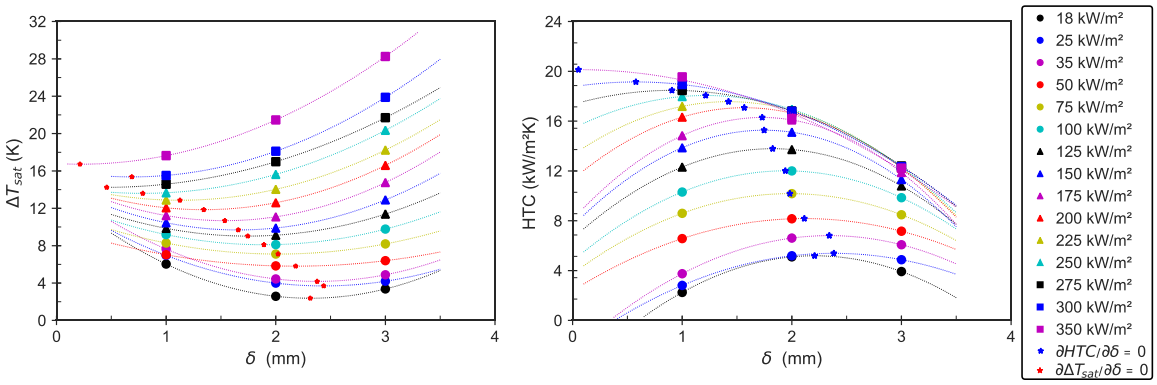

(a) (b)

Figure 15. Copper foam thickness variation: (a) Minimum superheating; (b) Maximum HTC.

As previously discussed, there is no constant value for optimum thickness. The optimum thickness varies with the heat fluxes and Fig. 15 shows the turning point for each heat flux. From maximum and minimum points, an inverse S-shaped curve,

$$\delta_{opt} = \frac{a}{b + \exp(c \cdot q'' - d)} \tag{19}$$

was fitted to find out the optimum thickness, δ_{opt}, as shown in Fig. 16.

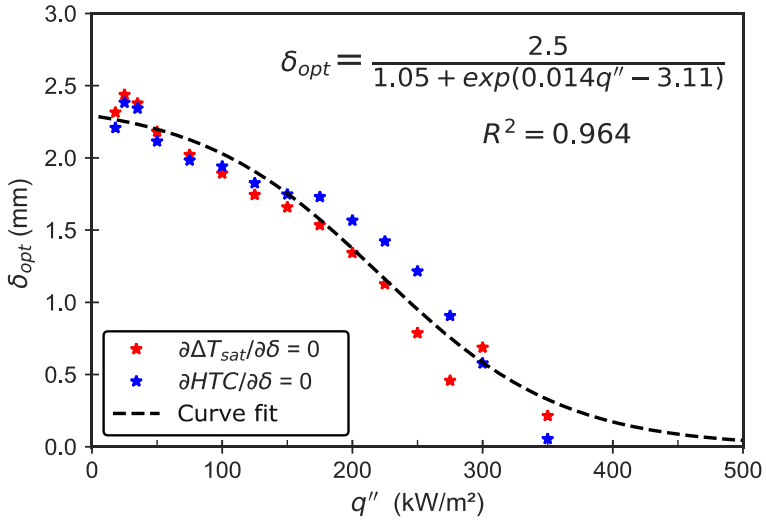

Figure 16. Copper foam optimum thickness for HFE-7100.

Obviously, the equation obtained in Fig. 16 works just for foams with similar characteristics of that showed in this work; however, the inverse S-shaped curve model is a good choice to fit other foams curves. First, it adjusts a maximum thickness for first heat fluxes where the larger wetted area combined with the natural convection plays a key role. Next, it shows the point where the vapor bubbles start to get trapped in the foam cell, and so, the thickness needs to be lower. Finally, it presents a minimum foam thickness higher than zero (thickness equal to zero means a plain surface where the performance is worst). In our study, the optimum thickness for heat fluxes in the range of 25 to 100 kW/m² is close to 2 mm, corroborating the inactive area for higher thickness as reported previously. For q'' > 100 kW/m², the optimum thickness decreases to values lower than 2 mm due to the trapping effect of the vapor bubbles.

4.3 *Vapor bubble dynamic visualization*

Bubbles dynamics were visualized by using a high-speed camera (Photron FASTCAM SA3) with a 1024 × 1024 maximum resolution and 1000 fps. Through videos and image tracking software, the bubble departure diameter (D_d) was calculated by averaging three diameter measurements immediately after the instant time that the bubble detached from the surface, as explained by Thiagarajan et al. [46]; for each heat flux the diameters were measured of at least three different sites during 1 second of recording. Figure 17 shows the bubble departure diameter for five heat flux values (from 10 to 25 kW/m²), including well-known correlations to validate the results for plain surfaces; the error bars are the standard deviation of measurement. Moreover, the data from Thiagarajan et al. [46] were plotted for comparison. It is worth mentioning that none of the correlations considered includes direct consideration of surface conditions: Fritz's correlation [42] takes into account a balance between buoyancy force and surface tension force; Cole and Rohsenow's correlation [47] correlated the bubble diameter departure at low pressures as a function of Jakob number by replacing the wall superheat by the liquid critical temperature; Borishanskiy et al. [48] used thermodynamic similitude to develop a correlation for the bubble departure diameter. The later predicts well the Thiagarajan et al. [45] data and the experimental data for the plain surface.

In the most recent correlation, Phan et al. [49] incorporate the influence of fluid properties and the buoyancy effect as Fritz [42], but also consider the energy factor as

the contribution of the wetting effects. However, as the correlation does not take into account the heating surface morphology, it is not possible to predict the bubble departure diameter for foams surface and compare it with the measured value.

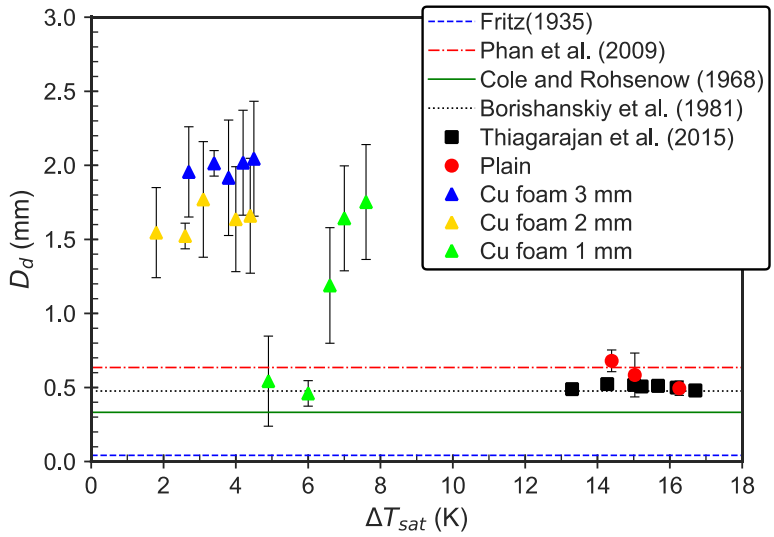

Figure 17. Bubble departure diameter distribution.

The nucleation sites on metal foams are activated at the first heat flux; for the highest foam thickness, small bubbles grow and coalescence within the foam structure leading the bubble departure diameter bigger than the other foams and plain surface. Such behavior decreases as the thickness also decreases for δ = 2 mm and δ = 1 mm. At the smallest thickness, the bubbles grow and departure in the first two heat fluxes; the mean bubble departure diameters are almost the same as the plain one. As heat flux increases, the bubble coalescence also increases, as a result, the mean D_d was close to the other foams. Figure 18 shows the pictures taken during the pool boiling and a schematic drawing in Fig. 19 complement the explanation above.

Plain	Cu foam 3 mm	Cu foam 2 mm	Cu foam 1 mm
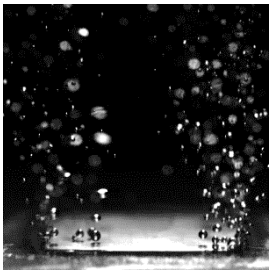	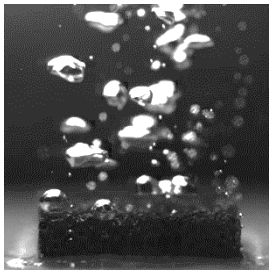	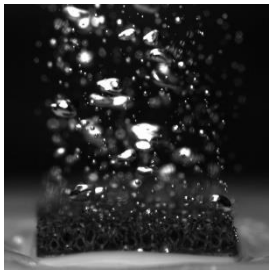	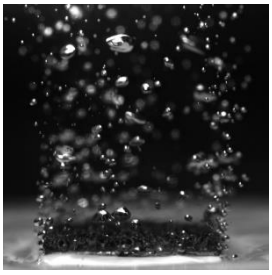
ΔT_{sat} =14.4 K	ΔT_{sat} = 3.8 K	ΔT_{sat} = 3.1 K	ΔT_{sat} = 6.6 K

Figure 18. Vapor bubbles visualization at low heat flux for plain and foams surfaces.

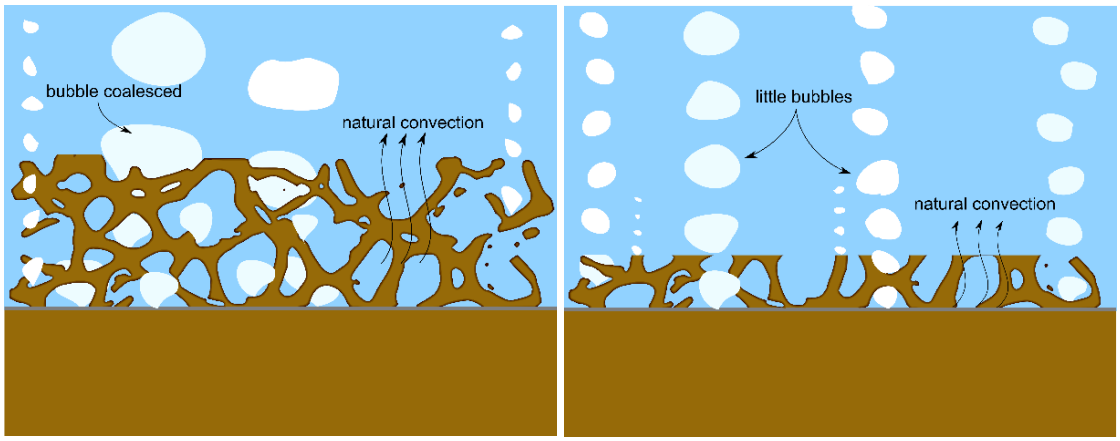

(a) (b)

Figure 19. Schematic drawing of vapor bubbles role on pool boiling at low heat flux for copper foam with: (a) 3 mm; (b) 1 mm in thickness.

As the heat flux increases, it is not possible to measure the bubble departure diameter; however, it is possible to compare the vapor bubbles patterns. Figure 20 shows vapor bubbles visualization at different heat flux values. At the highest foam thickness, the vapor bubbles start to flow not only in foam top but also at the foam lateral sides that difficult the liquid-vapor counterflow, decreasing the HTC. As foam thickness decreases the vapor bubbles concentrate at the foam top, which improves liquid replenishment in the porous matrix by the sides, Fig. 21.

Cu foam 3 mm	Cu foam 2 mm	Cu foam 1 mm
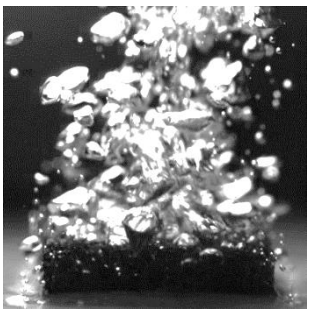	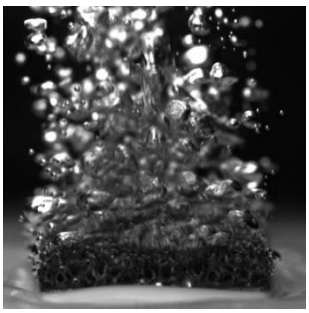	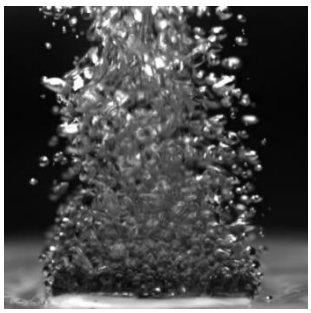
75 kW/m²	75 kW/m²	75 kW/m²
ΔT_{sat} = 8.2 K	ΔT_{sat} = 7.1 K	ΔT_{sat} = 8.3 K

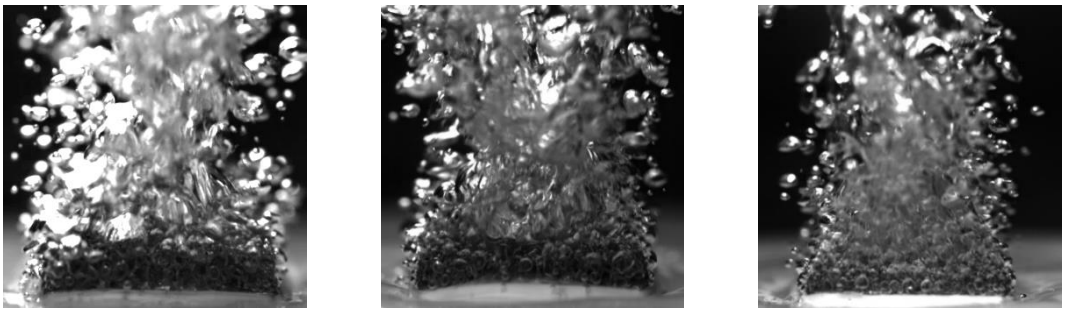

150 kW/m²	150 kW/m²	150 kW/m²
ΔT_{sat} = 12.9 K	ΔT_{sat} = 9.9 K	ΔT_{sat} = 10.5 K
250 kW/m²	250 kW/m²	250 kW/m²
ΔT_{sat} = 20.4 K	ΔT_{sat} = 15.6 K	ΔT_{sat} = 13.7 K
350 kW/m²	350 kW/m²	350 kW/m²
ΔT_{sat} = 28.3 K	ΔT_{sat} = 21.5 K	ΔT_{sat} = 17.6 K

Figure 20. Vapor bubbles pattern at different heat flux values.

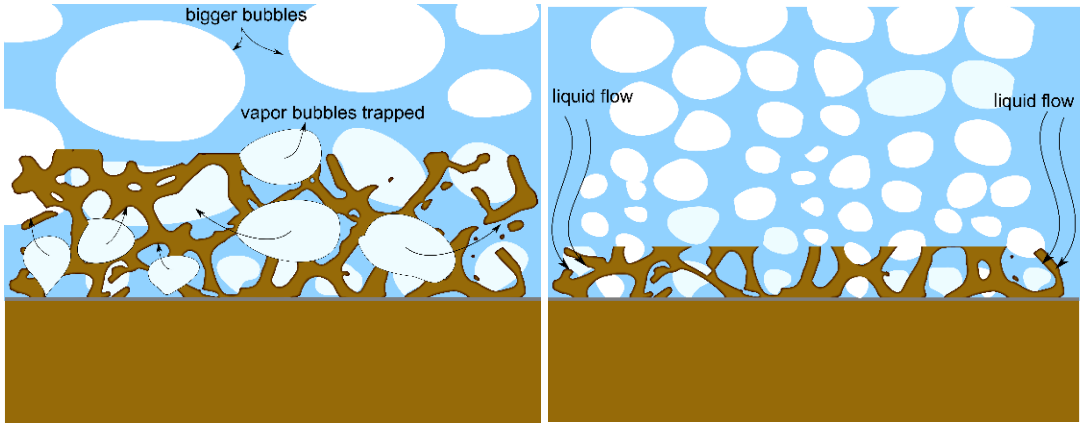

(a) (b)

Figure 21. Schematic drawing of vapor bubbles role on pool boiling at high heat flux with copper foam with: (a) 3 mm; (b) 1 mm in thickness.

4.4 *Summary of thickness foam influence on pool boiling*

By analyzing the effect foam thickness on pool boiling of HFE-7100 we noticed that there is an optimum thickness point for the first heat fluxes that is close to 2 mm, which eliminates the ONB overshoot and improves the HTC due to the bubbles nucleation (latent heat) and natural convection heat transfer. The thicker foam has an area that does not effectively contribute to heat transfer while the thinnest has a smaller area that mainly influences the natural convection heat transfer. By increasing the heat flux, the nucleation sites and bubble frequency also increase, leading to vapor bubbles to get trapped in the foam cell with higher thickness. It hinds the vapor flow on the foam top and the bubbles start to departure from the lateral sides, which difficult the liquid flow into the foam structure and decreases the vapor-liquid counterflow, deteriorating the HTC. Therefore, the lowest foam thickness reduces the entrapped vapor into the cell; additionally, the capillary-wicking ability increases and it also improves the HTC and the dryout heat flux due to prevention of hotspots within the foam surface. Figure 22 summarizes the foam thickness effect on pool boiling of HFE-7100.

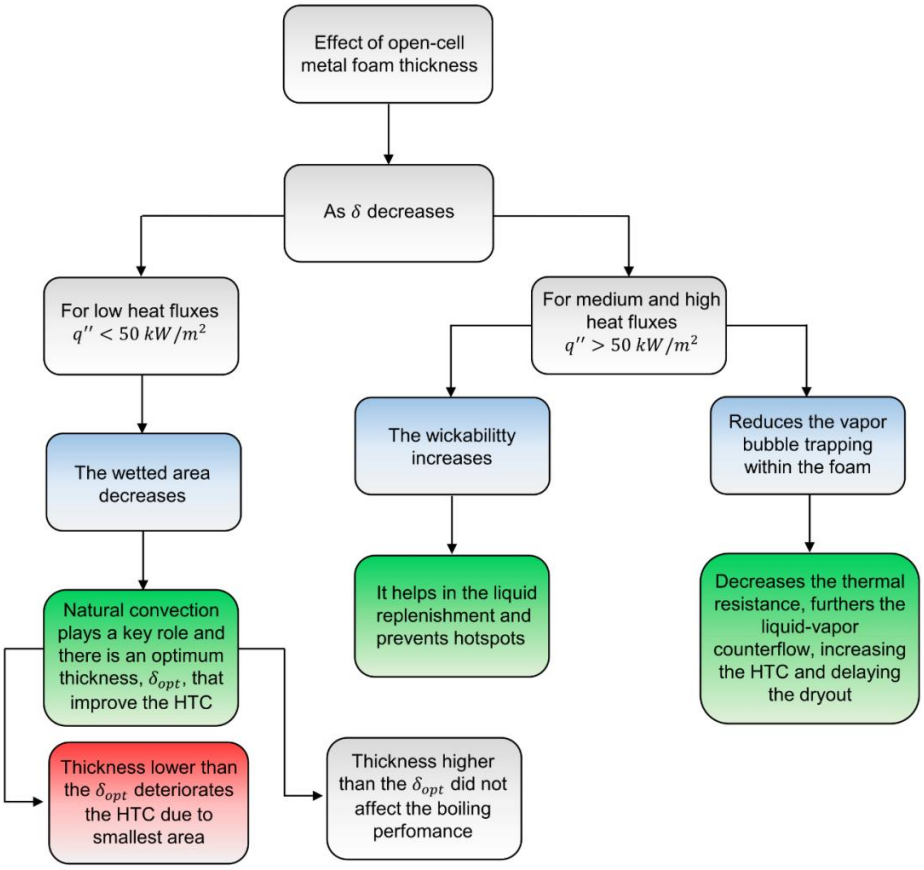

Figure 22. Effect of open-cell metal foam thickness on pool boiling of HFE-7100.

5. Conclusions

In this work, we presented a pool boiling experimental work by using HFE-7100, at saturation conditions, and copper foams of 1 mm, 2 mm, and 3 mm in thickness as the heating surface. The following conclusions can be drawn from the present study:

- ✓ The copper foams eliminated the thermal overshoot at the onset nucleate boiling, with some nucleation sites being activated at the first heat fluxes. It improves HTC due to the latent heat coupled with natural convection heat transfer.
- ✓ For heat fluxes lower than 200 kW/m², the 'Cu foam 2 mm' showed the greater HTC while for heat fluxes higher than 200 kW/m² the 'Cu foam 1 mm' is better; reaching an HTC 145 % higher than the plain one.
- ✓ There is no constant value for optimum thickness; in other words, the optimum thickness varies with the heat flux. In addition, the inverse S-shaped curve fitted well with our data and presented the optimum thickness variation with the heat flux.
- ✓ From bubbles visualization, it can be seen that small bubbles grew and coalescence within the foam structure leading the bubble departure diameter bigger than the other foams and plain surface. That behavior decreases as the thickness also decreases to $\delta = 2$ mm and $\delta = 1$ mm. As the heat flux increase, the vapor bubbles start to flow not only in foam top but also at the foam lateral sides that difficult the liquid-vapor counter flow and decrease the HTC while in the lowest thickness the vapor bubbles outlet concentrates at the foam top and allows the fresh liquid inlet at the lateral sides. Additionally, the capillary-wicking ability increases as the thickness decreases and it also improves the HTC and the dryout heat flux due to the prevention of hotspots within the foam surface.

Acknowledgments

The authors are grateful for the financial support from the PPGEM – UNESP/FEIS, from CAPES, from the National Council of Technological and Scientific Development of Brazil (CNPq grant number 458702/2014-5) and from FAPESP (grant number 2013/15431-7; 2017/13813-0; 2019/02566-8). A. S. Moita also acknowledges the contribution of FCT for financing her contract through the IF 2015 recruitment program

and associated exploratory project. We also extend our gratitude to Prof. Dr. Alessandro Roger Rodrigues and Prof. Dr. Tito José Bonagamba (Escola de Engenharia de São Carlos/EESC-USP) for their important contribution to this work.

References

[1] X.H. Yang, J. Liu, Advances in Liquid Metal Science and Technology in Chip Cooling and Thermal Management, *Advances in Heat Transfer*, vol. 50 Elsevier, 2018. DOI:10.1016/bs.aiht.2018.07.002.

[2] K.C. Leong, J.Y. Ho, K.K. Wong, A critical review of pool and flow boiling heat transfer of dielectric fluids on enhanced surfaces, Appl. Therm. Eng. 112 (2017) 999–1019. DOI:10.1016/j.applthermaleng.2016.10.138.

[3] M.S. El-Genk, Immersion cooling nucleate boiling of high power computer chips, Energy Convers. Manag. 53 (2012) 205–218. DOI:10.1016/j.enconman.2011.08.008.

[4] G. Liang, I. Mudawar, Review of pool boiling enhancement by surface modification, Int. J. Heat Mass Transf. 128 (2019) 892–933. DOI:10.1016/j.ijheatmasstransfer.2018.09.026.

[5] S.M. Sri-Jayantha, G. McVicker, K. Bernstein, J.U. Knickerbocker, Thermomechanical Modeling of 3D Packages., IBM J. Res. Dev. 52 (2008) 623–634. DOI:10.1147/JRD.2008.5388568.

[6] B. Agostini, M. Fabbri, J.E. Park, L. Wojtan, J.R. Thome, B. Michel, State of the art of high heat flux cooling technologies, Heat Transf. Eng. 28 (2007) 258–281. DOI:10.1080/01457630601117799.

[7] E. Teodori, A.S. Moita, A.L.N. MOREIRA, Empirical and modeling-based correlations for pool boiling on microstructured surfaces, Interfacial Phenom. Heat Transf. 2 (2014) 273–292. DOI:10.1615/InterfacPhenomHeatTransfer.2015011663.

[8] 3M product brochure, 3M Novec™ engineered fluid HFE-7100 for heat transfer, (2002).

[9] 3M product information, Fluorinert™ Electronic Liquid FC-72, (2000).

[10] S.A. Khan, N. Sezer, M. Koç, Design, fabrication and nucleate pool-boiling heat transfer performance of hybrid micro-nano scale 2-D modulated porous surfaces, Appl. Therm. Eng. 153 (2019) 168–180. DOI:10.1016/j.applthermaleng.2019.02.133.

[11] H. Seo, Y. Lim, H. Shin, I.C. Bang, Effects of hole patterns on surface temperature distributions in pool boiling, Int. J. Heat Mass Transf. 120 (2018) 587–596. DOI:10.1016/j.ijheatmasstransfer.2017.12.066.

[12] M. Shojaeian, A. Koşar, Pool boiling and flow boiling on micro- and nanostructured surfaces, Exp. Therm. Fluid Sci. 63 (2015) 45–73. DOI:10.1016/j.expthermflusci.2014.12.016.

[13] L. Lin, M.A. Kedzierski, Review of low-GWP refrigerant pool boiling heat transfer on enhanced surfaces, Int. J. Heat Mass Transf. 131 (2019) 1279–1303. DOI:10.1016/j.ijheatmasstransfer.2018.11.142.

[14] L.J. Gibson, M. F. Ashby, Cellular Solids: Structure and properties., Cambridge Solid State Science Series, 2nd ed., Cambridge University Press, 1997.

[15] C.Y. Zhao, Review on thermal transport in high porosity cellular metal foams with open cells, Int. J. Heat Mass Transf. 55 (2012) 3618–3632. DOI:10.1016/j.ijheatmasstransfer.2012.03.017.

[16] B. Athreya, R. Mahajan, S. Sett, Pool Boiling of FC-72 over Metal Foams: Effect of Foam Orientation and Geometry, In: 8th AIAA/ASME Jt. Thermophys. Heat Transf. Conf. (2002) 1–10. DOI:10.2514/6.2002-3214.

[17] J. Xu, X. Ji, W. Zhang, G. Liu, Pool boiling heat transfer of ultra-light copper foam with open cells, Int. J. Multiph. Flow. 34 (2008) 1008–1022. DOI:10.1016/j.ijmultiphaseflow.2008.05.003.

[18] Y. Yang, X. Ji, J. Xu, Pool boiling heat transfer on copper foam covers with water as working fluid, Int. J. Therm. Sci. 49 (2010) 1227–1237. DOI:10.1016/j.ijthermalsci.2010.01.013.

[19] Z.G. Xu, C.Y. Zhao, Thickness effect on pool boiling heat transfer of trapezoid-shaped copper foam fins, Appl. Therm. Eng. 60 (2013) 359–370. DOI:10.1016/j.applthermaleng.2013.07.013.

[20] Z.G. Xu, C.Y. Zhao, Experimental study on pool boiling heat transfer in gradient metal foams, Int. J. Heat Mass Transf. 85 (2015) 824–829. DOI:10.1016/j.ijheatmasstransfer.2015.02.017.

[21] L. Zhou, W. Li, T. Ma, X. Du, International Journal of Heat and Mass Transfer Experimental study on boiling heat transfer of a self-rewetting fluid on copper foams with pore-density gradient structures, Int. J. Heat Mass Transf. 124 (2018) 210–219. DOI:10.1016/j.ijheatmasstransfer.2018.03.070.

[22] K.K. Wong, K.C. Leong, Saturated pool boiling enhancement using porous lattice structures produced by Selective Laser Melting, Int. J. Heat Mass Transf. 121 (2018) 46–63. DOI:10.1016/j.ijheatmasstransfer.2017.12.148.

[23] M. F. Ashby, T. Evans, N. A. Fleck, J. W. Hutchinson, H. N. G. Wadley, L. J.. Gibson, Metal foams: a design guide. Elsevier, 2000.

[24] J. Banhart, Manufacture, characterization and application of cellular metals and metal foams, Prog. Mater. Sci. 46 (2001) 559–632. DOI: 10.1016/S0079-6425(00)00002-5

[25]M. P. Groover, Fundamentals of modern manufacturing: materials processes, and systems. John Wiley & Sons, 5th ed. 2012.

[26] Brun, E., Vicente, J., Topin, F., & Occelli, R., 2008. IMorph: A 3D morphological tool to fully analyze all kind of cellular materials. Cellular Metals for Structural and Functional Applications.

[27] J. Vicente, F. Topin, J.-V. Daurelle, Open Celled Material Structural Properties Measurement: From Morphology to Transport Properties, Mater. Trans. 47 (2006) 2195–2202. DOI:10.2320/matertrans.47.2195.

[28] S. Sarangi, J.A. Weibel, S. V. Garimella, Quantitative Evaluation of the Dependence of Pool Boiling Heat Transfer Enhancement on Sintered Particle Coating Characteristics, J. Heat Transfer. 139 (2016) 021502. DOI:10.1115/1.4034901.

[29] Y. Nam, S. Sharratt, C. Byon, S.J. Kim, Y.S. Ju, Fabrication and characterization of the capillary performance of superhydrophilic Cu micropost arrays, J.

Microelectromechanical Syst. 19 (2010) 581–588. DOI:10.1109/JMEMS.2010.2043922.

[30] H.S. Ahn, C. Lee, J. Kim, M.H. Kim, The effect of capillary wicking action of micro/nano structures on pool boiling critical heat flux, Int. J. Heat Mass Transf. 55 (2012) 89–92. DOI:10.1016/j.ijheatmasstransfer.2011.08.044.

[31] A.M. Gheitaghy, H. Saffari, D. Ghasimi, A. Ghasemi, Effect of electrolyte temperature on porous electrodeposited copper for pool boiling enhancement, Appl. Therm. Eng. 113 (2017) 1097–1106. DOI:10.1016/j.applthermaleng.2016.11.106.

[32] Y.Q. Wang, J.L. Luo, Y. Heng, D.C. Mo, S.S. Lyu, Wettability modification to further enhance the pool boiling performance of the micro nano bi-porous copper surface structure, Int. J. Heat Mass Transf. 119 (2018) 333–342. DOI:10.1016/j.ijheatmasstransfer.2017.11.080.

[33] H.S. Ahn, G. Park, J.M. Kim, J. Kim, M.H. Kim, The effect of water absorption on critical heat flux enhancement during pool boiling, Exp. Therm. Fluid Sci. 42 (2012) 187–195. DOI:10.1016/j.expthermflusci.2012.05.005.

[34] M.M. Rahman, E. Ölçeroglu, M. McCarthy, Role of wickability on the critical heat flux of structured superhydrophilic surfaces, Langmuir. 30 (2014) 11225–11234. DOI:10.1021/la5030923.

[35] Z. Cao, B. Liu, C. Preger, Z. Wu, Y. Zhang, X. Wang, M.E. Messing, K. Deppert, J. Wei, B. Sundén, Pool boiling heat transfer of FC-72 on pin-fin silicon surfaces with nanoparticle deposition, Int. J. Heat Mass Transf. 126 (2018) 1019–1033. DOI:10.1016/j.ijheatmasstransfer.2018.05.033.

[36] Z. Cao, Z. Wu, A.-D. Pham, Y. Yang, S. Abbood, P. Falkman, T. Ruzgas, C. Albèr, B. Sundén, Pool boiling of HFE-7200 on nanoparticle-coating surfaces: Experiments and heat transfer analysis, Int. J. Heat Mass Transf. 133 (2019) 548–560. DOI:10.1016/j.ijheatmasstransfer.2018.12.140.

[37] L. L. Manetti, T. S. Mogaji, P. A. Beck, E. M. Cardoso, Evaluation of the heat transfer enhancement during pool boiling using low concentrations of Al2O3 -water based nanofluid, Exp. Therm. Fluid Sci. 87 (2017) 191–200. DOI:10.1016/j.expthermflusci.2017.04.018.

[38] M.H. Rausch, L. Kretschmer, S. Will, A. Leipertz, A.P. Fröba, Density, surface tension, and kinematic viscosity of hydrofluoroethers HFE-7000, HFE-7100, HFE-7200, HFE-7300, and HFE-7500, J. Chem. Eng. Data. 60 (2015) 3759–3765. DOI:10.1021/acs.jced.5b00691.

[39] R.J. Moffat, Describing the Uncertainties in Experimental Results, (1988) 3–17.

[40] W. M. Rohsenow, A method of correlating heat transfer data for surface boiling of liquids. Transactions of ASME – J. Heat Transfer, Vol. 74, pp. 969-976 (1952).

[41] I. S. Kiyomura, T. S. Mogaji, L. L. Manetti, E. M. Cardoso, A predictive model for confined and unconfined nucleate boiling heat transfer coefficient, Appl. Therm. Eng. 127 (2017) 1274–1284. DOI:10.1016/j.applthermaleng.2017.08.135.

[42] Fritz, W. Berechnung des maximal volumes von dampfblasen. Physik Zeitschr, Vol. 36, pp. 379-384 (1935).

[43] G. Ribatski, J.M.S. Jabardo, Experimental study of nucleate boiling of halocarbon refrigerants on cylindrical surfaces, Int. J. Heat Mass Transf. 46 (2003) 4439–4451. DOI:10.1016/S0017-9310(03)00252-7.

[44] Stephan, K. Heat transfer in condensation and boiling: Springer-Verlag (1992).

[45] Z. Cao, Z. Wu, B. Sundén, Heat transfer prediction and critical heat flux mechanism for pool boiling of NOVEC-649 on microporous copper surfaces, Int. J. Heat Mass Transf. 141 (2019) 818–834. DOI:10.1016/j.ijheatmasstransfer.2019.07.036.

[46] S.J. Thiagarajan, R. Yang, C. King, S. Narumanchi, Bubble dynamics and nucleate pool boiling heat transfer on microporous copper surfaces, Int. J. Heat Mass Transf. 89 (2015) 1297–1315. DOI:10.1016/j.ijheatmasstransfer.2015.06.013.

[47] Cole, R., & Rohsenow, W. M. Correlation of bubble departure diameters for boiling of saturated liquids. In Chem. Eng. Prog. Symp. Ser, Vol. 65, pp. 211-213 (1968).

[48] Borishanskiy, A. V., Danilova, G. P., & Kupriyanova, A. V. Correlation of data on heat transfer in, and elementary characteristics of the nucleate boiling mechanism. Heat Transfer Sov. Res, Vol. 13, pp. 100-116 (1981).

[49] Phan, H. T., Caney, N., Marty, P., Colasson, S., & Gavillet, J. (2009). How does surface wettability influence nucleate boiling?. Comptes Rendus Mécanique, 337(5), 251-259. DOI: 10.1016/j.crme.2009.06.032